Application of Impedance Matching for Enhanced Transmitted Power in a Thermophotovoltaic System

Chungwei Lin, Bingnan Wang, and Koon Hoo Teo
Mitsubishi Electric Research Laboratories, 201 Broadway, Cambridge, Massachusetts 02139, USA

Prabhakar Bandaru
University of California San Diego, 9500 Gilman Drive, La Jolla, California 92093, USA
(Received 7 October 2016; revised manuscript received 2 December 2016; published 6 March 2017)

Based on the impedance-matching condition, we propose a few configurations that can greatly enhance radiation power transfer from the emitter to the photovoltaic (PV) cell for a near-field-based thermophotovoltaic system. In addition to the emitter and the PV cell, these configurations involve the use of additional materials that support resonant modes, such as a metallic material whose dielectric function can be described by a Drude model, or a dielectric material whose dielectric function can be approximated by a Lorentz oscillator model. We show that, by coating the PV cell on both the front and back sides with Lorentz materials, the transferred power can be 2.5 times larger than that without any decorations. When Drude metals are included in the configuration, the optimal transferred power can be 3 times larger than the system without additional materials. We find that the key to enhancing transmitted power is to place a thin layer of Drude or Lorentz material on the front side (facing the emitter) of the PV cell.

DOI: 10.1103/PhysRevApplied.7.034003

I. INTRODUCTION

Thermophotovoltaic (TPV) energy conversion is a process of converting heat into electricity via *photons* [1,2]. A basic TPV system consists of an emitter and a photovoltaic (PV) cell (also commonly referred to as a solar cell) [2–8]. The emitter is kept at a certain (high) temperature by a heat source, and it radiates photons to the PV cell. A PV cell is a semiconductor, characterized by a band gap E_g. When absorbing the emitter-radiated photons of energy larger than the band gap, electrons occupying the valence bands are excited to the conduction band and become sources of an electric current. Assuming each photon of energy larger than E_g generates an electron-hole pair in the PV cell, two fundamental factors governing the TPV efficiency are (1) the number of photons and (2) the (energy) spectrum of photons absorbed by the PV cell. For a given emitter radiation spectrum, photons of low and high energies cannot be fully converted into the electric current: the low-energy photons are wasted, as they cannot generate conducting electrons; the high-energy photons generate hot electrons which decay quickly to the conduction-band bottom (via emitting phonons), and the net voltage is, at most, $V_g = E_g/|e|$ [9]. The ideal emitter spectrum is, therefore, a narrow-width spectrum peaked slightly above the band gap, with peak intensity as strong as possible [2]. If achieved, the overall efficiency of a solar TPV system (where the Sun is the heat source of the emitter) can be as high as 85% [2], as compared to the Shockley-Queisser limit of 40% (with fully concentrated sunlight) [9].

For the far-field-based TPV system—where the distance between the emitter and the PV cell is much larger than the characteristic wavelength of the photon—the emission power at a given frequency is limited by the blackbody radiation. The ideal far-field-based design is to make the emitter emissivity zero for subgap photons, unity for above-gap photons. Approaches to achieve this goal include using photonic crystal [10–12], patterning the metallic surface [13–16], and combining metal and dielectric [17]. Generally, these approaches intend to reshape the photon density of state (DOS) of the *emitter* such that the DOS of subgap photons is small, while that of above-gap photons is large. One way to increase the emission power is to fill the space between the emitter and the PV cell with a medium of refractive index n, in which case the emission power is increased by n^2. The micron-gap TPV [18,19] is another implementation of this approach. There, the separation between the emitter and the PV cell is shortened so that the emission power is increased by n^2, with n being the refractive index of the PV cell itself.

For the near-field-based TPV system [6,7], the emitter supports a few (or at least one) resonant modes which are spatially localized, and the separation between the emitter and the PV cell is much shorter than the wavelength defined by the resonant modes. The near-field absorbed-radiation spectrum is peaked at the resonant energies, with the peak intensity a few orders higher than the blackbody limit [20]. This property fits perfectly with the ideal emitter requirement. Recently, based on the "impedance matching" derived from the coupled-mode theory (CMT) [21,22], Karalis and Joannopoulos proposed that one could *create*

resonances on the PV-cell side to further enhance the radiation energy transfer. Based on this principle, they were able to design system configurations that achieve the high (larger than 47%, depending on the actual geometries) heat-to-electricity efficiency [23].

In this work, we propose a few alternative configurations for a near-field TPV system, based on the impedance-matching condition, that can greatly enhance the radiation power transfer from the emitter to the PV cell. The building blocks of these configurations are materials whose dielectric function can be approximated by a Lorentz oscillator model [24], or metals whose dielectric function can be approximated by a Drude model. By coating the PV cell on both the front and back sides of the PV cell with Lorentz materials, the transferred power can be 2.5 times larger than that without any decorations. When Drude metals are used in the configuration, the transferred power can be 3 times larger than in the original system. We find that a key component for these alternative configurations is to place an additional thin layer of material on the front side (between the emitter and the PV cell) of the PV cell.

The rest of the paper is organized as follows. In Sec. II, we use a model system composed of Lorentz materials to illustrate our design principle. The process to quickly determine the parameters is also explained. In Sec. III, we apply the same design procedure to new configurations with Drude metals included. A few discussions and a brief summary are given in Sec. IV.

II. DESIGN PRINCIPLE AND MODEL CALCULATION

A. Radiation energy transfer, model materials, and design principle

We consider the materials arranged in a layered configuration [see Fig. 1(a) for an illustration]. In this case, the radiative heat transfer between materials can be computed using the dyadic Green's function [20,25–28] and the random current source obeying the fluctuation-dissipation theorem [29]. For the planar structure, where the in-plane momentum $\mathbf{K}$ (which defines the x-y plane) is a good quantum number, the Poynting vector normal to the plane as a function z has the form

$$S_z(z) = \int_0^\infty \frac{d\omega}{2\pi}\hbar\omega[\Theta_i(\omega)-\Theta_j(\omega)]\frac{A}{(2\pi)^2}\int d^2\mathbf{K}\varepsilon(\omega,\mathbf{K};z)$$
$$\frac{S_z}{A} = \int_0^\infty \frac{d\omega}{2\pi}\hbar\omega[\Theta_i(\omega)-\Theta_j(\omega)]\frac{(2\pi)}{(2\pi)^2}\int kdk\varepsilon(\omega,k;z). \quad (1)$$

Here, $\Theta_i(\omega) = [e^{\hbar\omega/(k_B T_i)}-1]^{-1}$ is the Planck distribution, A is the surface area of the emitter, k_B is the Boltzmann constant, $k = |\mathbf{K}|$, and $\varepsilon(\omega,k;z)$ is a dimensionless function determined by the spatial configuration. We compute

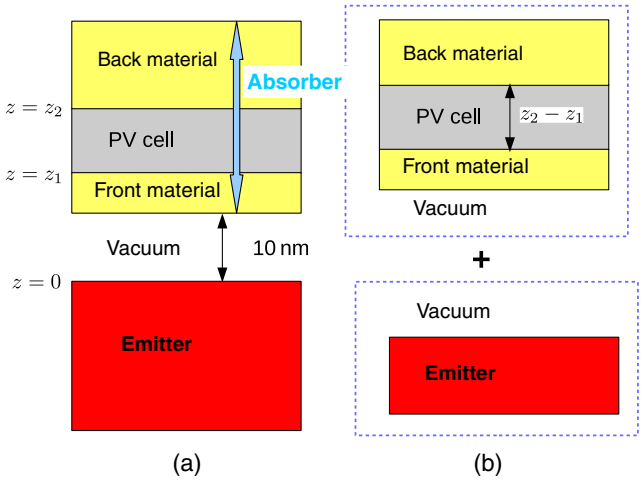

FIG. 1. (a) The general layered configurations considered in this paper. The emitter occupies the $z < 0$ region, whereas the PV cell occupies $z_1 < z < z_2$. We put some materials adjacent to the PV cell (on either or both sides) for the impedance matching, and the combined materials above the vacuum form the absorber. The separation between the emitter and the absorber is fixed at 10 nm in our model consideration. (b) For impedance matching, we consider the resonant energies for the bottom emitter–vacuum and top vacuum–absorber subsystems separately.

Eq. (1) exactly, and the detailed expression can be found in several references [26–28]. For the layered configurations, we consider the emitter occupying the $z < 0$ space, and the PV cell occupying $z_1 < z < z_2$. The radiation power per unit area absorbed by the PV cell is given by $\{[S_z(z_1)]/A\} - \{[S_z(z_2)]/A\}$.

As a model calculation, we consider the emitter whose dielectric function can be described by the Lorentz oscillator model corresponding to boron nitride [20] as

$$\epsilon_L(\omega) = \epsilon_\infty \frac{\omega^2 - \omega_{\mathrm{LO}}^2 + i\gamma\omega}{\omega^2 - \omega_{\mathrm{TO}}^2 + i\gamma\omega},$$

with $\epsilon_\infty = 4.46$. ω_{LO} and ω_{TO} are frequencies of longitudinal and transverse optical modes. All frequencies are measured in $\omega_{\mathrm{LO}} = \bar{\omega}_{\mathrm{LO}} \equiv 0.1616$ eV, with $\omega_{\mathrm{TO}}/\bar{\omega}_{\mathrm{LO}} = 0.81$, $\gamma/\bar{\omega}_{\mathrm{LO}} = 0.0041$. We also define $\bar{k}_{\mathrm{LO}} = \bar{\omega}_{\mathrm{LO}}/c$, and we scale all momentums with respect to it. For the PV cell, the dielectric function is governed by the direct valence-to-conduction interband transition [30,31].

$$\epsilon_{\mathrm{PV}}(\omega) = \epsilon_r(\omega) + i\epsilon_i(\omega)$$
$$\epsilon_i(\omega) = \begin{cases} A\sqrt{x-1}/x^2, & x > 1 \\ 0, & x < 1 \end{cases}$$
$$\epsilon_r(\omega) = \begin{cases} B + A(2-\sqrt{1+x})/x^2, & x > 1 \\ B + A(2-\sqrt{1+x}-\sqrt{1-x})/x^2, & x < 1 \end{cases},$$

with $x = \hbar\omega/E_g$. As a model calculation, we use $[A, B, E_g/(\hbar\bar{\omega}_{\mathrm{LO}})] = (6, 10, 0.804)$ [20]. This corresponds to a hypothetical semiconductor of a small gap of 0.13 eV (for example, a few-layer black phosphorous with adatoms [32]). We vary A and B between 1 and 15, the typical values extracted from Refs. [30,31], and find that varying A and B within this range does not change our conclusion. Using the dielectric function, all photons of sufficient energies absorbed by the PV cell are used to generate the electron-hole pairs, and we comment on the effects of other lossy mechanisms in Sec. IV.

We are free to put other materials next to the PV cell, either in front of the PV cell (labeled "front material"), behind the PV cell (labeled "back material"), or on both sides; the whole combination, including the PV cell and the front material or the back material or both, is referred to as an "absorber." We fix the distance between the emitter and the absorber to be 10 nm, and the goal is to maximize the radiation power absorbed by the PV cell alone $[\{[S_z(z_1)]/A\} - \{[S_z(z_2)]/A\}$ in Eq. (1)], *not* by the whole absorber.

We now describe the design principle and how to practically search for the optimal parameters. According to the CMT analysis, the radiation energy transfer between the emitter and the absorber originates from their coupling to the common resonant modes of the *whole* system [22,24]. If only the emitter-vacuum subsystem sustains a resonant mode, then the design principle is to make the system resonance have the decay rate to the emitter as close as possible to the decay rate to the absorber. This impedance-matching condition maximizes the radiation energy transfer [22,33]. As the decay rate is related to the loss and is more difficult to control, we do not consider optimizing the system of single resonance. If both the emitter-vacuum and vacuum-absorber subsystems sustain their respective resonant mode (so that there are two resonant modes of the whole system), the maximum radiation transfer happens when the real-part complex eigenenergies of these two subsystems are close in value for the largest possible $\mathbf{K}$ range [34], which serves as the design principle. One sees that a symmetric emitter-vacuum-emitter configuration automatically satisfies this criterion, i.e., the emitter-vacuum and vacuum-emitter eigenvalues are identical for the entire range of $\mathbf{K}$. As shown in Ref. [20], the radiation power transfer in the symmetric configuration is about 100 times larger than that of the asymmetric configuration. In practice, we first consider the bottom emitter–vacuum and top vacuum–absorber subsystems separately [see Fig. 1(b)], and we solve the eigenenergies for each in-plane momentum $\mathbf{K}$, employing the condition used in calculating the surface-plasmon dispersion [24,35,36]. We then tune the parameters so that the eigenvalues of both subsystems are close for the widest range of $\mathbf{K}$. We apply this principle to asymmetric configurations in the following subsections.

B. PV cell with a front or back material

In this subsection, one additional material is placed on one side of a PV cell for impedance matching. The reference system is an emitter-vacuum-PV configuration. Similar to the emitter, the additional material is again assumed to have a Lorentzian dielectric function as in Eq. (II A), but with different LO and TO frequencies. For simplicity, we assume that the ratio of LO and TO frequencies of the added material is fixed at 0.81, and we vary the LO frequency to maximize the radiation energy transfer. Under this assumption, a material is characterized by its LO frequency only. In the calculation, we fix the emitter temperature at 1000 K, and the absorber at 300 K.

We first consider the case where the added material is placed on the back side of the PV cell, with the thickness of the PV cell fixed at 10 nm [see Fig. 2(a)]. Therefore, the absorber is composed of the PV cell and a back material. By doing so, one resonant mode is created at the absorber side, and the total power (per area) absorbed by the PV cell is increased by about 39% compared to the reference emitter–vacuum (10 nm)–PV configuration [see Fig. 2(b)]. From Fig. 2(c), we see that, for a wide range of k, the (upper) absorber resonant energy is smaller than the (lower) emitter resonant energy. This result is expected, as the PV cell provides a dielectric environment that screens the Coulomb interaction and thus lowers the surface resonant energy of the PV cell or back material (with the back material being chosen as the emitter here) [37]. As shown in Fig. 2(d), when we choose the back material such that its ω_{LO} is 1.12 times larger than that of the emitter ($\omega_{\mathrm{LO}} = 1.12\bar{\omega}_{\mathrm{LO}}$), a very wide range of k's have identical resonant energies, implying a larger radiation energy transfer. As shown in Fig. 2(b), this choice indeed increases the total PV absorbed power (per area) by 73%.

We go on to consider the case where the additional material is placed on the front side of a PV cell, and the thickness of the PV cell is semi-infinite [see Fig. 3(a)]. In this case, the front material is chosen to be the same material as the emitter, as this is close to the symmetric configuration. Since our purpose is to increase the power absorbed by the PV cell, the front material cannot be too thick; otherwise, the front material would absorb all the radiation. As shown in Fig. 3(b), the optimal thickness of the front material is around 4 nm, where the absorbed power per area is increased by 89% compared to the reference system.

C. PV cell with both front and back materials

We can also add materials to both sides [see Fig. 4(a)] of a PV cell for the impedance matching. The material choice is based on the results in the previous subsection. The front material is chosen to be the same as the emitter, whereas the back material is either the same as the emitter or the one whose LO frequency is 1.12 times larger than that of the emitter [Fig. 2(d)]. The reason for choosing the emitter

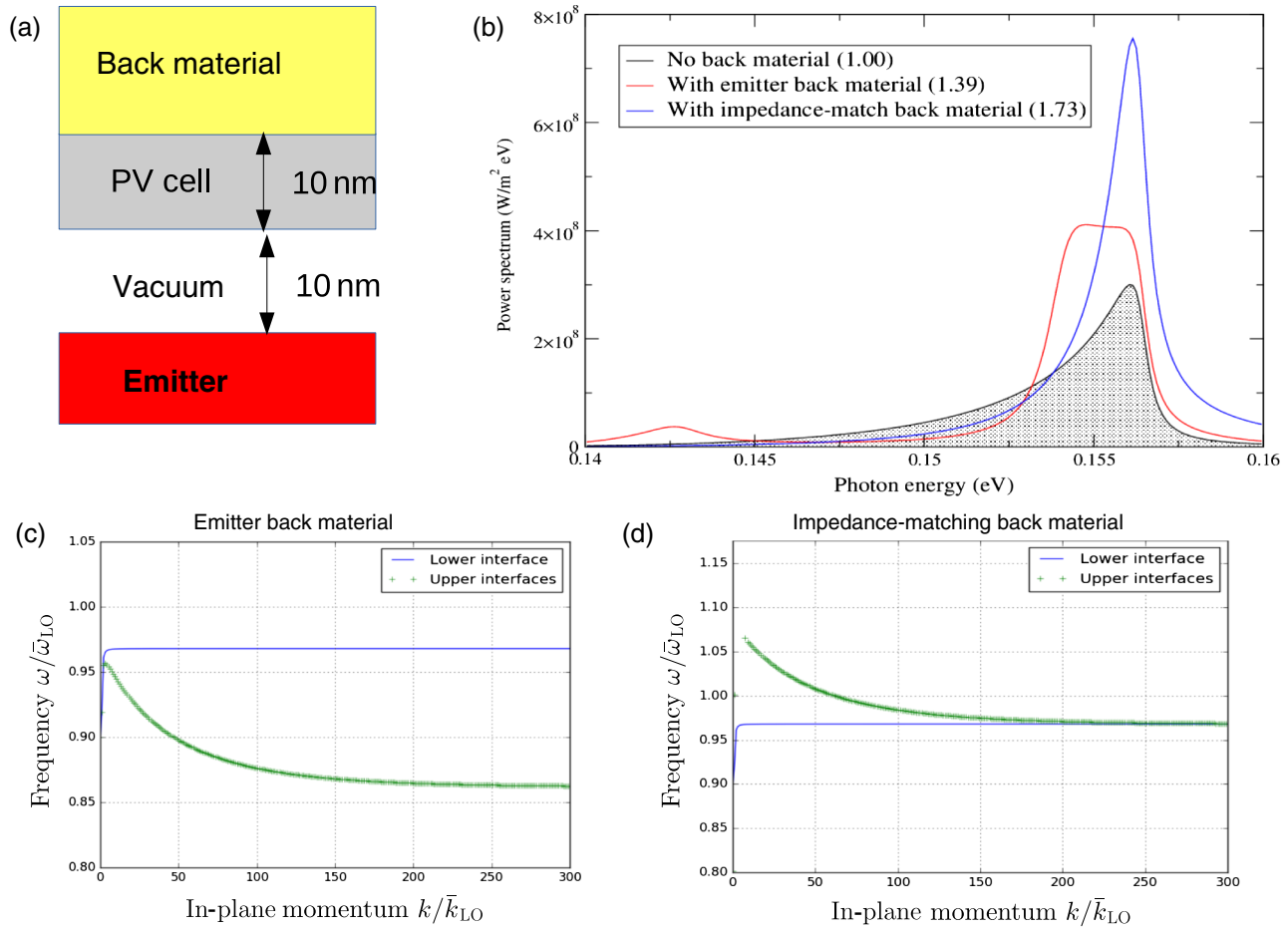

FIG. 2. (a) Illustration of the emitter–vacuum (10 nm)–PV–back material configuration. The vacuum gap is 10 nm, and the PV thickness is 10 nm when there is a back material and is semi-infinite when there is no back material. (b) The radiation power spectrum *absorbed* by the PV cell and the ratio of the integrated spectrum are given in parentheses, with the emitter-vacuum-PV configuration taken as the reference (the shaded region). When the back material is the same as the emitter, the total power per area is increased by 39%. When the back material is chosen so that its $\omega_{\rm LO}$ is 1.12 times larger than that of the emitter, the total power per area is increased by 73%. (c),(d) The real part of the eigenenergies for bottom and top subsystems. (c) The back material is the emitter. (d) The back material whose $\omega_{\rm LO}$ is 1.12 times larger than that of the emitter. When they are close in values over a wide momentum space, the impedance matching is better fulfilled, resulting in a larger radiation power transfer.

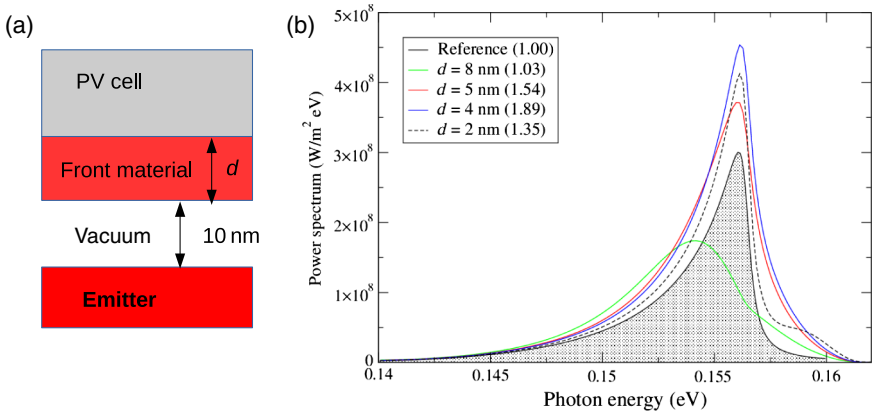

FIG. 3. (a) Illustration of the emitter–vacuum (10 nm)–front material–PV configuration. The vacuum gap is 10 nm, and the PV thickness is semi-infinite. (b) The radiation power spectrum absorbed by the PV cell and the ratio of integrated spectrum are given in parentheses, with the emitter-vacuum-PV configuration taken as the reference (the shaded region). The front material is chosen to be the same as the emitter, and there exists an optimal thickness—around 4 nm—where the PV absorbed power is maximized.

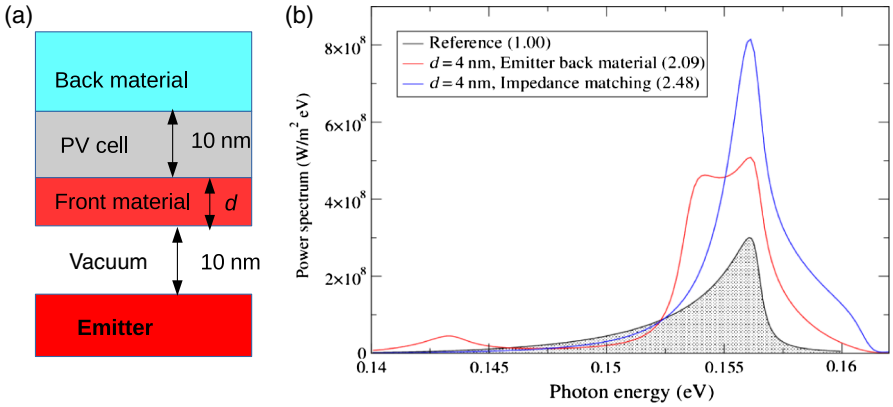

FIG. 4. (a) Illustration of the emitter–vacuum (10 nm)–front material (the emitter)–PV–back material configuration. The vacuum gap and the PV thickness are 10 nm. The front material is the same as the emitter. (b) The radiation power spectrum absorbed by the PV cell and the ratio of the integrated spectrum are given in parentheses, with the emitter-vacuum-PV configuration taken as the reference (the shaded region). Two types of back materials are chosen: the same material as the emitter and the one with impedance matching that is shown in Fig. 2(d). The front-material thickness is 4 nm, corresponding to the maximum radiation energy transfer.

material as the back material is that, in practice, one may not be able to find the desired material for exact impedance matching. As shown in Fig. 4(b), for both choices, the absorbed power by the PV cell is at least twice as large as that of the reference configuration. When the impedance-matching condition is satisfied (the ω_{LO} of the back material is 1.12 times larger than the emitter), the absorbed power for the PV cell can be 2.5 times larger than for the reference system.

III. METAL EMITTER AND HYBRIDS

Refractory-metal-based emitters are commonly used in TPV systems for high-temperature operation in TPV systems. In this section, we consider the metal emitters whose dielectric function can be approximated by the Drude model and repeat the analysis presented in Sec. II. For the Drude model, the dielectric function is

$$\epsilon_m = 1 - \frac{\omega_{\mathrm{pl}}^2}{\omega^2 + i\gamma_m\omega}. \tag{2}$$

For the metal emitter, we choose $\omega_{\mathrm{pl}} = \bar{\omega}_{\mathrm{pl}} = \sqrt{2} \times 0.97\bar{\omega}_{\mathrm{LO}}$, and $\gamma_m = 0.002\omega_{\mathrm{pl}}$. In the following discussion, different metals are characterized only by the different plasmon frequencies. From a static Coulomb consideration [35,36], the metal-vacuum interface supports a momentum-independent resonant mode of $0.97\bar{\omega}_{\mathrm{LO}}$, which is close to the value of the Lorentz model we use in the previous section [Fig. 2(c)]. We consider how to increase the radiation power transfer from the emitter by the metal-coated PV cells. The reference now is the metal–vacuum (10 nm)–PV configuration.

We first consider the case where the added metal is placed on the back side of the PV cell, as shown in Fig. 5(a). Similar to the procedure described in the previous section, we vary the plasma frequency of the back metal for impedance matching. By solving the eigenvalues of the top subsystem, we find that when the plasma frequency of the back metal is 2.6 times that of the emitter, the resonant modes of the two subsystems are close in value for a wide range of momentum values at high k [similar to Fig. 2(d), not shown]. Figure 5(b) shows the radiation power spectrum absorbed by the PV cell for back metals of various plasma frequencies. We indeed see that when the impedance-matching condition is satisfied, the maximum radiation energy—which is about 1.73 times larger than the reference system—is transferred.

We go on to consider the case where the added metal is placed on the front side of the PV cell, and the thickness of the PV cell is semi-infinite [see Fig. 5(c)]. For the same reason discussed in Sec. II B, we use the emitter as the front metal, and there exists an optimal thickness for radiation energy transfer to the PV cell. As shown in Fig. 5(d), the optimal thickness is around 5 nm, and the radiation energy transfer can be 2.16 times larger than in the reference system.

When metals can be added on both sides, the transferred radiation energy is further increased. Based on the results of a one-side addition, the front metal is chosen to be the same as the emitter, with a thickness of 5 nm. We consider three different back materials, the emitter material, the Drude metal whose plasma frequency is 2.6 times that of the emitter, and a Lorentz material given in Fig. 2(d). The results are shown in Fig. 6. All three choices further increase the radiation energy absorbed by the PV cell. The largest radiation power transfer (3.5 times larger than the reference system) is achieved using the Drude metal whose plasma frequency is 2.6 times that of the emitter, as the impedance-matching condition is satisfied. We note that, in the present context, metal is used as a back material mainly to provide additional resonant modes that enhance the radiation transfer, and it is less relevant to its large reflectivity that prevents photon leakage. The latter effect can also increase the efficiency [2].

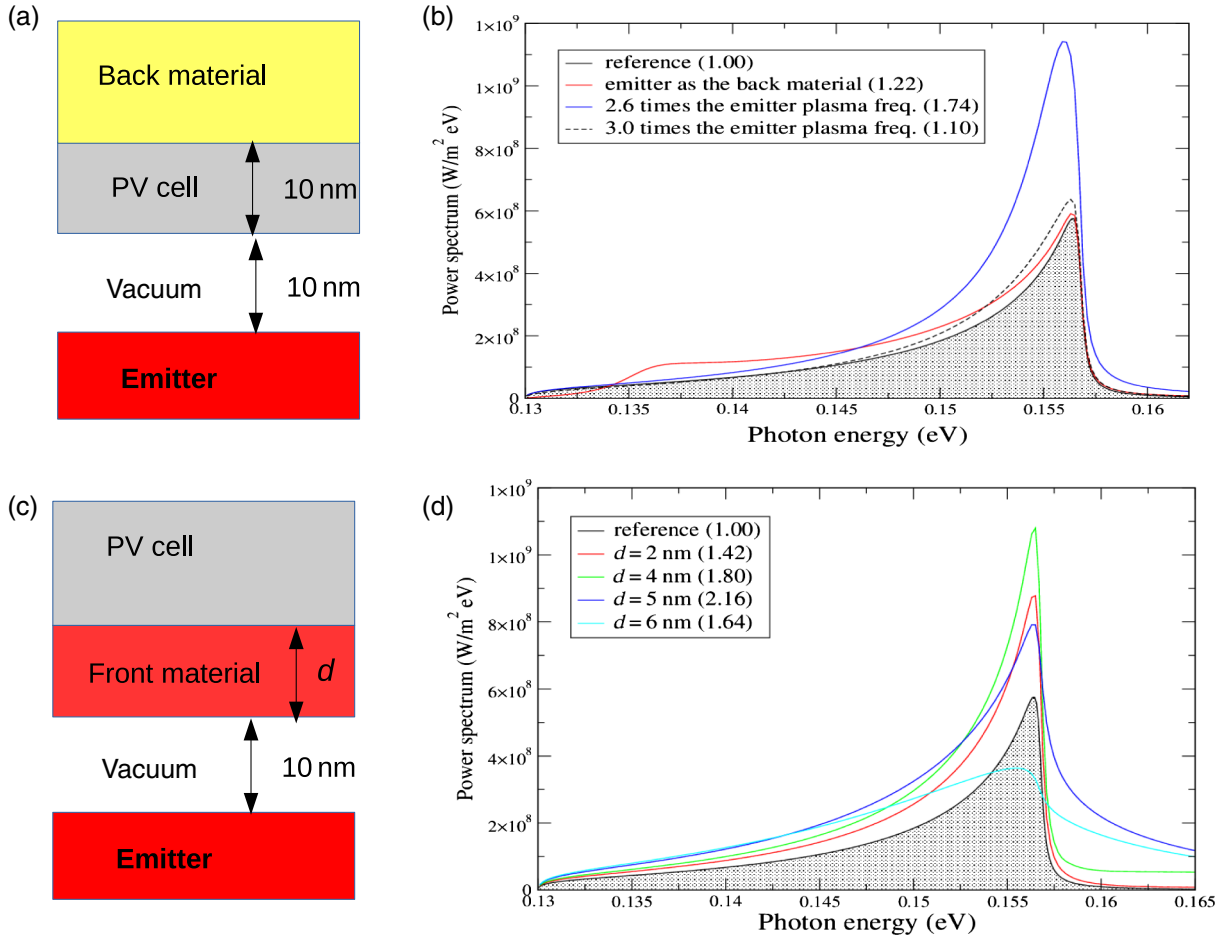

FIG. 5. (a) Illustration of the emitter–vacuum (10 nm)–PV–back material configuration. The vacuum gap is 10 nm and the PV thickness is 10 nm when there is a back material, and it is semi-infinite when there is no back material. (b) The radiation power spectrum absorbed by the PV cell, and the ratio of the integrated spectrum is given in parentheses, with the emitter-vacuum-PV configuration taken as the reference (the shaded region). When using the emitter as the back material, the total power per area is increased by 22%. When using the impedance-matching back material (the blue line; the metal plasma frequency is about 2.6 times that of the emitter), the total power per area is increased by 74%. (c) Illustration of the emitter–vacuum (10 nm)–front material–PV configuration. The vacuum gap is 10 nm, and the PV thickness is semi-infinite. (d) The radiation power spectrum absorbed by the PV cell and the ratio of integrated spectrum are given in parentheses, with the emitter-vacuum-PV configuration taken as the reference (the shaded region). The front material is chosen to be the same as the emitter, and there exists an optimal thickness—around 5 nm—where the PV absorbed power is maximized.

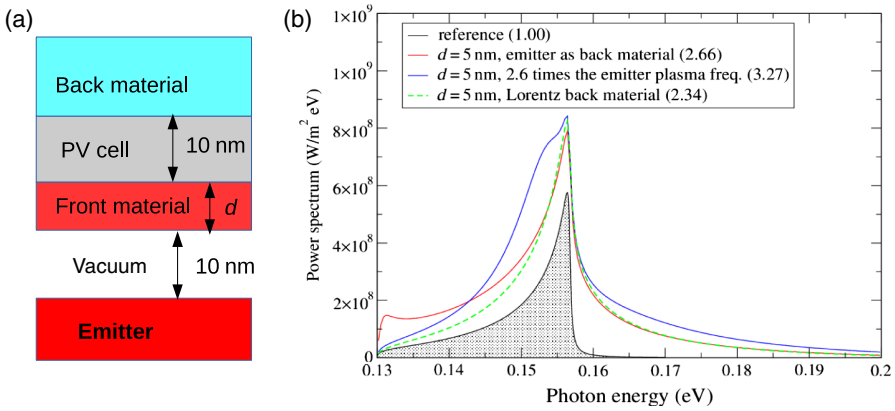

FIG. 6. (a) Illustration of the emitter–vacuum (10 nm)–front material (the emitter)–PV–back material configuration. The vacuum gap and the PV thickness are 10 nm. The front material is the same as the emitter. (b) The radiation power spectrum absorbed by the PV cell and the ratio of the integrated spectrum are given in parentheses, with the emitter-vacuum-PV configuration taken as the reference (the shaded region). Two types of back materials are chosen: the same material as the emitter and the one with impedance matching that is shown in Fig. 2(d). The front material thickness is 5 nm, corresponding to the maximum radiation energy transfer.

IV. DISCUSSION AND CONCLUSION

We now discuss our simulation results. First, we comment on the loss mechanisms inside the PV cell, which are important [23] but are not included in the model. As we model the PV cell only by the interband transition, the radiation power absorbed by the PV cell is assumed to generate conducting electrons only. When the absorbed radiation power is increased, the resulting electric output power also increases by the same ratio. Including lossy mechanisms inside the PV cell (such as the free-carrier absorption) means that some of the absorbed radiation energy is not used to generate conducting electrons. As the lossy mechanisms happen for both reference and designed configurations, we expect the increasing *ratio* of the PV absorbed radiation power and the increasing ratio of the corresponding output electric power between the designed configuration and the reference are still approximately unchanged. Second, for both Lorentz and metal additions, our calculations suggest placing a thin layer of emitter material on the front greatly increases the radiation power absorbed by the PV cell. This configuration may be counterintuitive, as adding a front material *increases* the distance between the PV cell and the emitter. However, the configuration can be understood straightforwardly from the CMT analysis, as the energy transfer is most efficient when the resonant energies of the emitter and the absorber are close for a wide range of in-plane momentum, and this gain in energy transfer outweighs the photon absorptions by the thin front material. One can further increase the radiation power transfer by placing a material on the back side of the PV cell, and the choice of the back material is such that the resonant energy of the absorber (the PV cell and the additions) is close to that of the emitter-vacuum subsystem. A combination of the front "emitter material" and back "impedance-matching material" gives the maximum radiation energy absorbed by the PV cell. If the impedance-matching back material cannot be found, using the emitter as the back material also helps considerably (more than 30%). Finally, we emphasize that the key physics of coating the PV cell is to *introduce* resonant modes to the absorber, with its resonant energy as close to the emitter-vacuum resonant energy as possible. From this perspective, one could try to introduce resonant modes by coating the PV cell with nanoparticles (with geometry and size chosen for impedance matching) or some two-dimensional materials, which can be another potential route to increase the radiation power transfer.

To conclude, we use the impedance matching condition, derived from the coupled-mode theory, to design the emitter-absorber configurations that maximize the near-field radiative heat transfer from the emitter to the PV cell of a TPV system. The procedure includes (i) separating the system into two subsystems with an emitter only and an absorber only, (2) finding the (complex) eigenvalues of each subsystem, and (iii) choosing parameters such that the eigenvalue difference between the subsystems is as small as possible for the largest possible range of in-plane momentum. As the procedure requires only eigenvalues, not eigenvectors, it is relatively fast and, if convenient, can be obtained by the time-domain solver. We find that by adding chosen materials of a Lorentzian dielectric function on both sides of the PV cell, the absorbed power by the PV cell can be 2.5 times larger than that of the basic emitter-vacuum-PV configuration. Our studies illustrate that the CMT analysis is indeed very valuable in determining the material parameters for near-field-based TPV designs, and it can be applied to various materials.

ACKNOWLEDGMENTS

We thank Zhuomin Zhang for the insightful comments and Jian-Jian Wang for the helpful discussions. P. R. Bandaru would like to acknowledge financial support form the National Science Foundation (CBET Award: 1606192).

[1] Peter Würfel, *Physics of Solar Cells* (Wiley-VCH, Weinheim, 2005).
[2] Nils-Peter Harder and Peter Würfel, Theoretical limits of thermophotovoltaic solar energy conversion, Semicond. Sci. Technol. **18**, S151 (2003).
[3] P. A. Davies and A. Luque, Solar thermophotovoltaics: Brief review and a new look, Sol. Energy Mater. Sol. Cells **33**, 11 (1994).
[4] Peter Bermel, Michael Ghebrebrhan, Walker Chan, Yi Xiang Yeng, Mohammad Araghchini, Rafif Hamam, Christopher H. Marton, Klavs F. Jensen, Marin Soljačić, John D. Joannopoulos, Steven G. Johnson, and Ivan Celanovic, Design and global optimization of high-efficiency thermophotovoltaic systems, Opt. Express **18**, A314 (2010).
[5] Andrej Lenert, David M. Bierman, Youngsuk Nam, Walker R. Chan, Ivan Celanović, Marin Soljacic, and Evelyn N. Wang, A nanophotonic solar thermophotovoltaic device, Nat. Nanotechnol. **9**, 126 (2014).
[6] S. Basu and Z. M. Zhang, Ultrasmall penetration depth in nanoscale thermal radiation, Appl. Phys. Lett. **95**, 133104 (2009).
[7] T. J. Bright, L. P. Wang, and Z. M. Zhang, Performance of near-field thermophotovoltaic cells enhanced with a back-side reflector, J. Heat Transfer **136**, 062701 (2014).
[8] David M. Bierman, Andrej Lenert, Walker R. Chan, Bikram Bhatia, Ivan Celanović, Marin Soljacic, and Evelyn N. Wang, Enhanced photovoltaic energy conversion using thermally based spectral shaping, Nat. Energy **1**, 16068 (2016).
[9] William Shockley and Hans J. Queisser, Detailed balance limit of efficiency of *p-n* junction solar cells, J. Appl. Phys. **32**, 510 (1961).
[10] Francis OSullivan, Ivan Celanovic, Natalija Jovanovic, John Kassakian, Shoji Akiyama, and Kazumi Wada, Optical characteristics of one-dimensional Si/SiO_2 photonic crystals for thermophotovoltaic applications, J. Appl. Phys. **97**, 033529 (2005).
[11] Marian Florescu, Hwang Lee, Irina Puscasu, Martin Pralle, Lucia Florescu, David Z. Ting, and Jonathan P. Dowling,

Improving solar cell efficiency using photonic band-gap materials, Sol. Energy Mater. Sol. Cells **91**, 1599 (2007).
[12] Jeremy N. Munday, The effect of photonic bandgap materials on the Shockley-Queisser limit, J. Appl. Phys. **112**, 064501 (2012).
[13] Koray Aydin, Vivian E. Ferry, Ryan M. Briggs, and Harry A. Atwater, Broadband polarization-independent resonant light absorption using ultrathin plasmonic super absorbers, Nat. Commun. **2**, 517 (2011).
[14] Hitoshi Sai, Yoshiaki Kanamori, and Hiroo Yugami, High-temperature resistive surface grating for spectral control of thermal radiation, Appl. Phys. Lett. **82**, 1685 (2003).
[15] Yi Xiang Yeng, Michael Ghebrebrhan, Peter Bermel, Walker R. Chan, John D. Joannopoulos, Marin Soljai, and Ivan Celanovic, Enabling high-temperature nanophotonics for energy applications, Proc. Natl. Acad. Sci. U.S.A. **109**, 2280 (2012).
[16] Jonathan K. Tong, Wei-Chun Hsu, Yi Huang, Svetlana V. Boriskina, and Gang Chen, Thin-film thermal well emitters and absorbers for high-efficiency thermophotovoltaics, Sci. Rep. **5**, 10661 (2015).
[17] Wei Gu, Guihua Tang, and Wenquan Tao, High efficiency thermophotovoltaic emitter by metamaterial-based nanopyramid array, Opt. Express **23**, 30681 (2015).
[18] R. DiMatteo, P. Greiff, D. Seltzer, D. Meulenberg, E. Brown, E. Carlen, K. Kaiser, S. Finberg, H. Nguyen, J. Azarkevich, P. Baldasaro, J. Beausang, L. Danielson, M. Dashiell, D. DePoy, H. Ehsani, W. Topper, K. Rahner, and R. Siergiej, Microngap thermophotovoltaics (MTPV), AIP Conf. Proc. **738**, 42 (2016).
[19] R. S. DiMatteo, P. Greiff, S. L. Finberg, K. A. YoungWaithe, H. K. H. Choy, M. M. Masaki, and C. G. Fonstad, Microngap thermophotovoltaics (MTPV), AIP Conf. Proc. **653**, 232 (2016).
[20] Arvind Narayanaswamy and Gang Chen, Surface modes for near field thermophotovoltaics, Appl. Phys. Lett. **82**, 3544 (2003).
[21] Linxiao Zhu, Sunil Sandhu, Clayton Otey, Shanhui Fan, Michael B. Sinclair, and Ting Shan Luk, Temporal coupled mode theory for thermal emission from a single thermal emitter supporting either a single mode or an orthogonal set of modes, Appl. Phys. Lett. **102**, 103104 (2013).
[22] Aristeidis Karalis and J. D. Joannopoulos, Temporal coupled-mode theory model for resonant near-field thermophotovoltaics, Appl. Phys. Lett. **107**, 141108 (2015).
[23] Aristeidis Karalis and J. D. Joannopoulos, Squeezing near-field thermal emission for ultra-efficient high-power thermophotovoltaic conversion, Sci. Rep. **6**, 141108 (2016).
[24] Chungwei Lin, Bingnan Wang, and Koon Hoo Teo, "Application of coupled mode theory on radiative heat transfer between layered insulating materials" (to be published).
[25] S. M. Rytov, Y. A. Kravtsov, and V. I. Tatarski, *Principles of Statistical Radiophysics*, Vol. 3 (Springer, Berlin, 1987).
[26] D. Polder and M. Van Hove, Theory of radiative heat transfer between closely spaced bodies, Phys. Rev. B **4**, 3303 (1971).
[27] A. A. Maradudin and D. L. Mills, Scattering and absorption of electromagnetic radiation by a semi-infinite medium in the presence of surface roughness, Phys. Rev. B **11**, 1392 (1975).
[28] Karl Joulain, Jean-Philippe Mulet, Franois Marquier, Rmi Carminati, and Jean-Jacques Greffet, Surface electromagnetic waves thermally excited: Radiative heat transfer, coherence properties and Casimir forces revisited in the near field, Surf. Sci. Rep. **57**, 59 (2005).
[29] Herbert B. Callen and Theodore A. Welton, Irreversibility and generalized noise, Phys. Rev. **83**, 34 (1951).
[30] D. E. Aspnes and A. A. Studna, Dielectric functions and optical parameters of Si, Ge, GaP, GaAs, GaSb, InP, InAs, and InSb from 1.5 to 6.0 eV, Phys. Rev. B **27**, 985 (1983).
[31] Sadao Adachi, Model dielectric constants of GaP, GaAs, GaSb, InP, InAs, and InSb, Phys. Rev. B **35**, 7454 (1987).
[32] Jimin Kim, Seung Su Baik, Sae Hee Ryu, Yeongsup Sohn, Soohyung Park, Byeong-Gyu Park, Jonathan Denlinger, Yeonjin Yi, Hyoung Joon Choi, and Keun Su Kim, Observation of tunable band gap and anisotropic Dirac semimetal state in black phosphorus, Science **349**, 723 (2015).
[33] Shanhui Fan, Wonjoo Suh, and J. D. Joannopoulos, Temporal coupled-mode theory for the Fano resonance in optical resonators, J. Opt. Soc. Am. A **20**, 569 (2003).
[34] For the top vacuum-absorber subsystem, the eigenenergy is obtained including only the damping processes in the PV cell.
[35] E. N. Economou, Surface plasmons in thin films, Phys. Rev. **182**, 539 (1969).
[36] E. N. Economou and K. L. Ngai, in *Advances in Chemical Physics*, Vol. 27, edited by I. Prigogine and S. A. Rice (John Wiley & Sons, New York, 1974), p. 265.
[37] The same effect happens at the metal-dielectric interface, as the plasma frequency is given by $\omega_{\mathrm{pl}}/\sqrt{1+\epsilon_{\mathrm{gap}}}$, with ω_{pl} being the bulk plasma frequency and ϵ_{gap} the dielectric constant of the "gap medium," which we take to be the vacuum here. Neglecting the retardation effect, the surface plasma frequency ω_{sp} is momentum independent and occurs at $\epsilon(\omega_{\mathrm{sp}}) = -\epsilon_{\mathrm{gap}}$.